THE JOURNAL OF BIOLOGICAL CHEMISTRY VOL. 288, NO. 48, pp. 34767–34776, November 29, 2013

Structural Basis of Substrate Conversion in a New Aromatic Peroxygenase

*CYTOCHROME P450 FUNCTIONALITY WITH BENEFITS**

Received for publication, August 28, 2013, and in revised form, October 2, 2013 Published, JBC Papers in Press, October 14, 2013, DOI 10.1074/jbc.M113.514521

Klaus Piontek[‡1], Eric Strittmatter[‡2], René Ullrich[§], Glenn Gröbe[¶], Marek J. Pecyna[§], Martin Kluge[§], Katrin Scheibner[¶], Martin Hofrichter[§], and Dietmar A. Plattner[‡3]

From the [‡]Institute of Organic Chemistry, University of Freiburg, Albertstrasse 21, 79104 Freiburg, the [§]Department of Bio- and Environmental Sciences, International Graduate School of Zittau, Markt 23, 02763 Zittau, and the [¶]Faculty of Natural Sciences, Department of Biotechnology, Lausitz University of Applied Sciences, Grossenhainer Strasse 57, 01968 Senftenberg, Germany

Background: Aromatic peroxygenases (APOs) are the "missing link" between heme peroxidases and P450-monooxygenases.
Results: Based on two crystal structures the substrate conversion of APOs is elucidated.
Conclusion: The specific design of the heme cavity and the distal heme access channel govern substrate specificity.
Significance: APOs can be utilized in biotechnology and organic synthesis having significant advantages when compared with cytochrome P450 enzymes.

Aromatic peroxygenases (APOs) represent a unique oxidoreductase sub-subclass of heme proteins with peroxygenase and peroxidase activity and were thus recently assigned a distinct EC classification (EC 1.11.2.1). They catalyze, *inter alia*, oxyfunctionalization reactions of aromatic and aliphatic hydrocarbons with remarkable regio- and stereoselectivities. When compared with cytochrome P450, APOs appear to be the choice enzymes for oxyfunctionalizations in organic synthesis due to their independence from a cellular environment and their greater chemical versatility. Here, the first two crystal structures of a heavily glycosylated fungal aromatic peroxygenase (AaeAPO) are described. They reveal different pH-dependent ligand binding modes. We model the fitting of various substrates in AaeAPO, illustrating the way the enzyme oxygenates polycyclic aromatic hydrocarbons. Spatial restrictions by a phenylalanine pentad in the active-site environment govern substrate specificity in AaeAPO.

Unfunctionalized hydrocarbons are the least reactive organic molecules and as such rather unfavorable reactants for organic syntheses. A straightforward functionalization method, however, would make them the ideal low cost precursor molecules for further synthetic transformations. Accordingly, this task has been singled out as one of the "Holy Grails" in chemistry (1, 2). Although considerable efforts have been made to develop selective methods for hydrocarbon functionalization, no generally applicable procedure has been established yet (3, 4). Combining several desirable properties such as specificity, practicability, environmental friendliness, and cost-effectiveness in one single catalytic system remains a long known Herculean task in chemistry, especially in hydrocarbon functionalization.

Nature's principal catalysts to mediate oxyfunctionalization are monooxygenases, among which cytochromes P450 represent the largest and most diverse group (5, 6). They incorporate oxygen from O_2 or, to a lesser degree, peroxides into various hydrocarbons with remarkable regio- and stereoselectivity (7). Major drawbacks for biotechnological applications, however, are the limitation to a cellular environment due to their dependence on external electron supply (NADPH/flavin reductases) and the issue of catalyst aging. The rapid decrease of activity in P450s results from their low stability caused by, for example, the tendency to lose the heme group upon conformational changes (8). Oxyfunctionalization systems based on aromatic peroxygenases (APOs),[4] however, do not suffer from these disadvantages. As secreted fungal enzymes, they act independently from the cellular environment, and thus no cell disruption is needed for isolation. Further, they utilize solely hydrogen peroxide as co-substrate and show no dependence on additional co-enzymes. Finally, due to their high degree of glycosylation, they are quite stable and soluble in aqueous environments (9).

APOs are extracellular heme thiolate enzymes found in true fungi (Eumycota) and fungus-like Chromalveolata (Oomycota) (10). The first APO, AaeAPO, was discovered in the widely cultivated agaric basidiomycete *Agrocybe aegerita*, commonly

* This work was supported by a grant from the Commission of the European Communities (to K. P. and M. H.), within a project of the 6th European Framework Programme (BIORENEW Contract NMP2-CT-2006-026456) and a grant through the 7th European Framework Programme (PEROXICATS Contract KBBE-2010-4-265397) (to M. H.). This work was also supported by the German Ministry of Education and Research (Bundesministerium für Bildung und Forschung) within the program "BioIndustrie 2021-Cluster Integrierte Biotechnologie 2021" (Project 0315877 to K. P., K. S., M. H., and D. A. P.).

The atomic coordinates and structure factors (codes 2YP1 and 2YOR) have been deposited in the Protein Data Bank (http://wwpdb.org/).

[1] To whom correspondence may be addressed. E-mail: Klaus.Piontek@ocbc.uni-freiburg.de.

[2] Supported by the International Research Training Group (IRTG) 1038 "Catalysts and Catalytic Reactions for Organic Synthesis" (CCROS) of the Deutsche Forschungsgemeinschaft (DFG).

[3] To whom correspondence may be addressed. E-mail: Dietmar.Plattner@chemie.uni-freiburg.de.

[4] The abbreviations used are: APO, aromatic peroxygenase; 4MI, 4(5)-methylimidazole; Aae, *A. aegerita*; ACT, acetate; CPO, chloroperoxidase; ICP-OES, inductively coupled plasma optical emission spectroscopy; Mro, *Marasmius rotula*; MZ0, 4(5)-(hydroxymethyl)imidazole; PAH, polycyclic aromatic hydrocarbon.

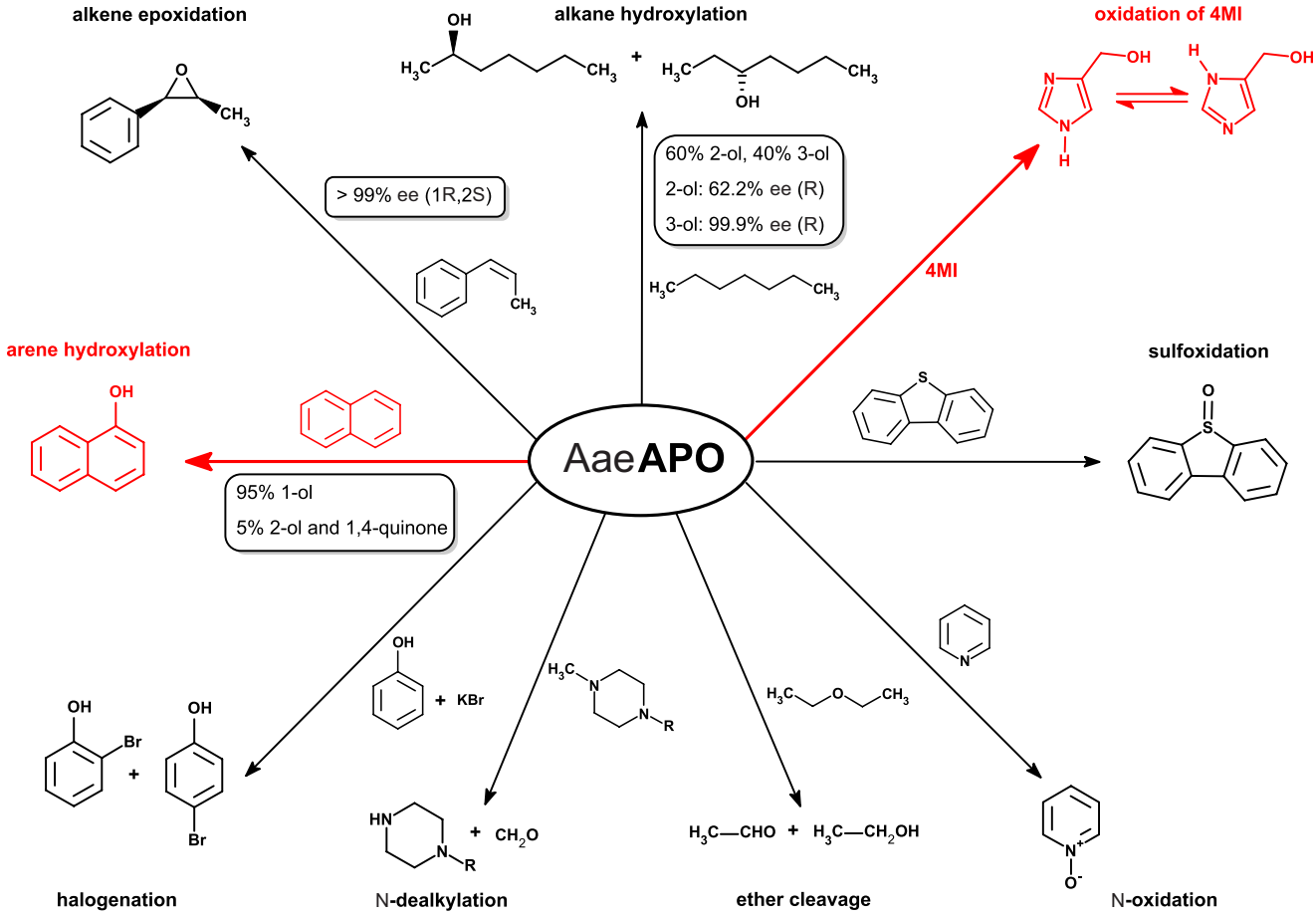

FIGURE 1. **Selected reactions catalyzed by AaeAPO.** Each reaction is illustrated by a typical example. The reactions discussed in this study are marked in *red*.

known as black poplar mushroom, and was initially regarded as a haloperoxidase (11). AaeAPO is able to catalyze the oxidation of veratryl alcohol, a classic substrate to monitor lignin peroxidase activity (11). Further organic substrates of AaeAPO, both aromatics as well as aliphatics, were identified in close succession (10, 12). AaeAPO turned out to be an accomplished catalyst for chemo- and stereoselective reactions, for example for the introduction of oxygen into hydrocarbons (10, 12–14). Alkanes such as heptane are hydroxylated in the 2- and the 3-positions with enantiomeric excesses up to 99.9% (Fig. 1). The enantioselectivity of alkane hydroxylation achieved with AaeAPO surpasses that of P450 oxygenases by far (12). Its catalytic versatility has been demonstrated for various substrates, such as naphthalenes, toluene, ethylbenzene, alkanes, alkenes, and saturated as well as unsaturated fatty acids (10, 14). Besides oxygenation of carbon atoms, AaeAPO also catalyzes the *N*- and *S*-oxidation of heterocycles (pyridine, dibenzothiophene) and the cleavage of ethers as well as of secondary and tertiary amines (10, 15). In addition, the enzyme displays a halogenating activity, although much less pronounced than fungal chloroperoxidase (CPO) and limited to an unspecific bromination of CH activated substrates (10). Enzyme-based routines suggest themselves for "green" organic synthesis because they operate in mild, environmentally friendly conditions. In fact, fungal oxidoreductases have recently been applied in various organic transformations, notably in the synthesis of drug metabolites (16).

Polycyclic aromatic hydrocarbons (PAHs), and related compounds such as dibenzothiophene (Fig. 1), are infamous environmental pollutants. They are found in crude oil, coal, and their refined products and are eventually emitted during technical processes (petroleum refining, coal tar distillation, combustion) (17). Additionally, PAHs are elements of exhaust gases and factory effluents and are linked with serious health issues; benzo[*a*]pyrene, as an example, is directly involved in carcinogenesis (18). APOs, through oxyfunctionalization, alter the chemical properties, and thereby the ecotoxicological and physiological effects of PAHs, *e.g.* by solubilization. PAH-derived alcohols and quinones can be covalently incorporated in humic substances, which is tantamount to their detoxification for other organisms (19).

Due to their catalytic versatility and broad substrate range, APOs were assigned a distinct classification as "unspecific peroxygenases" by the Nomenclature Committee of the International Union of Biochemistry and Molecular Biology (NC-IUBMB) (EC 1.11.2.1). A screening of public sequence databases revealed about 1,000 homologous nucleotide sequences encoding putative heme-thiolate peroxidases/peroxygenases in fungi with the exception of yeast (10). In addition to AaeAPO, to date the APOs of the ink cap *Coprinellus radians* and of the

pinwheel mushroom *Marasmius rotula* (MroAPO) have also been isolated and characterized (20). They show relatively low sequence homology with respect to AaeAPO, 65% between AaeAPO and MroAPO, and differ mainly in terms of their substrate range and catalytic efficiency.

A distant relative of APOs is CPO (21, 22), which can be considered a functional hybrid between heme peroxidases and cytochrome P450. The sequence identity between CPO and AaeAPO is barely 30%, but nonetheless larger than any homology between APOs and other heme enzymes such as lignin peroxidase and cytochrome P450. We approached the crystal structure determination of AaeAPO to supply a structural basis for its remarkable catalytic properties. As no search model for molecular replacement was available, its structure was solved by single-wavelength anomalous dispersion using the heme iron as the single anomalous scatterer (23). Two crystal forms grown at different pHs were subsequently analyzed. One of these structures contains an organic molecule identified as 4(5)-(hydroxymethyl)imidazole (MZ0), the presence of which can be explained by the oxidation of its precursor 4(5)-methylimidazole (4MI) stemming from the growth medium. The latter has been associated with carcinogenesis and was shown to induce tumors within the lower respiratory tract (alveoles, bronchi) of mice (24). It was therefore recently added to the list of the International Agency for Research on Cancer (IARC) as an agent "*possibly cancerogenic to humans (Group 2B*)."

We present an in-depth study of the structural characteristics of this new subclass of peroxidases. The binding modes for several substrates were scrutinized by docking experiments of aromatic compounds. Substrate specificities of APOs are determined by a clamp collar-like phenylalanine pentad at the distal heme site of AaeAPO and the variation thereof in other APOs.

EXPERIMENTAL PROCEDURES

Fungal Cultivation, Protein Purification, Crystallization, X-ray Data Collection, Processing, and Structure Solution—Experimental details of the cultivation of *A. aegerita*, the purification, crystallization, and x-ray data collection of AaeAPO-MZ0 (MZ0 = 4(5)-(hydroxymethyl)imidazole) and AaeAPO-ACT (ACT = acetate), as well as the structure solution of AaeAPO-MZ0 were published elsewhere (23). In summary, fungal cultures were grown at 297 K in a stirred tank bioreactor. The culture liquid was collected, filtrated, and concentrated. Subsequently, the crude AaeAPO preparation was further purified to a homogeneous molecular weight by three steps of fast protein liquid chromatography (FPLC) using SP Sepharose, Mono Q, and Mono S columns. The fraction of the most abundant isoenzyme was concentrated, dialyzed against 10 mM sodium acetate buffer, stored at 277 K, and subsequently used for crystallization experiments. N-terminal sequencing of 10 amino acids was performed by Edman degradation at Prot@gen AG, Dortmund, Germany.

Purified AaeAPO in 10 mM sodium acetate, pH 6.0, was used for crystallization screens applying the kits Crystal Screen 1 (Hampton Research) and Screen 6 (Jena Bioscience) using the hanging-drop vapor diffusion technique. Initial crystallization conditions were improved by refinement of pH, precipitant, and protein concentration. Large single crystals could be produced with drops of 10 and 20 μl applying the hanging- and sitting-drop technique, respectively. For crystals obtained at pH 8.5 and 4.6 with ammonium sulfate as precipitant, native x-ray data were collected on the macromolecular crystallographic beam line ID23-1 at the European Synchrotron Radiation Facility (ESRF) (Grenoble, France) at cryogenic temperatures. For AaeAPO-MZ0, additional multiwavelength anomalous diffraction data at the iron edge (at peak, high energy remote and inflection wavelengths) were recorded. Attempts to utilize the anomalous signal of the reportedly bound manganese were unsuccessful. X-ray fluorescence spectroscopy did to not show any signal for Mn^{2+}. Data were recorded on a Q315R Area Detector Systems Corp. charge-coupled device detector and processed and scaled with the XDS program package (25, 26). Both crystal forms diffracted initially to 1.8–2.0 Å resolution, but resolution rapidly decreased during data collection. High quality data sets were obtained to 2.1 and 2.3 Å resolution for AaeAPO-MZ0 and AaeAPO-ACT, respectively. The AaeAPO-MZ0 crystal structure was solved with the single-wavelength anomalous dispersion method because only a limited portion of the data collected with the radiation at the peak wavelength was useful due to radiation damage. A two-site substructure (the two heme iron atoms in the asymmetric unit) was obtained using SHELXD (27, 28), and the correct hand was found with SHELXE using data up to 4 Å resolution. Improvement of the phasing could be achieved by further refinement of the heavy atom sites in autoSHARP (29) and subsequent density modifications using SOLOMON (30). This process, performed using data up to 3 Å resolution, indicated two complete molecules, but the resulting map was untraceable. Further density modification (including noncrystallographic symmetry averaging) and phase extension up to 2.52 Å resolution within autoSHARP yielded an interpretable electron density. A first partial model was obtained with Buccaneer (31) and preliminarily refined in REFMAC5 (32). Subsequent rounds of manual model building in COOT (33) and refinement in REFMAC5 eventually resulted in a well behaved AaeAPO-MZ0 model. The AaeAPO-ACT crystal structure was solved with molecular replacement using the AaeAPO-MZ0 structure as search model with the program PHASER (34) and further improved as described above. The refinement statistics are summarized in Table 1. Model images were generated using PyMOL (35) and HOLLOW (36).

TABLE 1
Refinement statistics of AaeAPO crystal structures

	Crystal	
	AaeAPO-MZ0	AaeAPO-ACT
Resolution range (Å)[a]	47.51-2.19 (2.25-2.19)	48.91-2.31 (2.31-2.37)
R_{work}/R_{free}[b]	16.9 (40.4)/23.7 (45.0)	17.74 (22.4)/23.04 (33.3)
Total no. of non-H-atoms	6,261	12,291
No. of water molecules	643	1,186
No. of carbohydrates	34	59
Mean B-factors (Å^2)	23.3	29.9
Iron cation	9.20	19.9
Magnesium cation	9.13	19.3
r.m.s.[c] deviations (Å)		
Bonds (Å)	0.017	0.010
Angles (°)	1.617	1.206

[a] Values for the highest shell in parentheses.
[b] R_{free} calculated with 5% of the data.
[c] r.m.s., root mean square.

Determination of the Metal Content in AaeAPO by Optical Emission Spectroscopy (OES)—Purified enzyme was washed with sodium acetate buffer (10 mM) and diluted with distilled water (1:50) to give a 3 μM protein solution as determined by a standard Bradford assay. Inductively coupled plasma optical emission spectroscopy (ICP-OES) and ICP mass spectrometry (ICP-MS) were performed on an Optima 3000 system and an Elas DRC-e device (both from PerkinElmer Inc.), respectively. The OES system was calibrated with the "ICP multi-element standard solution IV" (magnesium, potassium, calcium, manganese, iron, copper) as well as the "phosphorus ICP standard" (both from Merck, Darmstadt, Germany) in 1 and 10 mg/liter concentrations and deionized water as blank solution. Measurements were performed according to the manufacturers' specifications. Different concentrations (2, 15, and 50 μg/liter) of the "ICP multi-element standard solution VI" (vanadium, manganese, iron, cobalt, copper) (Merck) were used to calibrate the MS unit.

Ligand Docking Experiments—Ligand docking was performed using the Molegro Virtual Docker software (37). The "expanded van der Waals" algorithm with a grid size of 0.5 Å was employed to identify the ligand binding cavities. Each experiment included 50 cycles using the respective PAH or 4MI molecule as ligand. The population size was set to 200 over a radius of 12 Å around the predicted binding cavity with a grid size of 0.2 Å. For each position, 10,000 iterations were performed. Clustering of similar positions was enabled by using a root mean square deviation of 1.5 Å.

Tracing of 4MI in the Growth Medium, Its Extraction, and Conversion—20 g of soybean meal (Hensel Vollsoja; Schoeneberger GmbH, Magstadt, Germany) was extracted overnight using 500 ml of boiling methanol in a Soxhlet apparatus. After removal of the solvent with a rotary evaporator, the residue was redissolved in a small amount of methanol. The polar molecules were then extracted applying an ion pair extraction protocol (38); the crude extract was mixed with 4 ml 0.2 M Na_3PO_4 buffer, pH 6, and vortexed for 30 s. After centrifugation (7 min, 3,500 $\times$ *g*), 5 ml of 0.1 M bis-2-ethylhexyl-phosphate in $CHCl_3$ was applied. The solution was shaken shortly and centrifuged again for 3 min at 5,000 $\times$ *g*. The organic phase was separated and acidified with 4 ml of 0.1 M HCl. Electrospray mass ionization mass spectra were recorded on a Finnigan-MAT TSQ-7000 mass spectrometer.

The oxidative conversion of 4MI was followed by HPLC using an Agilent Series 1200 system (Agilent, Waldbronn, Germany) equipped with a Nucleodur 100 5 NH_2 RP column (Macherey-Nagel, Düren, Germany), 150 $\times$ 4.6 mm. Conversion of 4MI was performed using 1 mM 4MI, 2 mM H_2O_2, and 2 units ml^{-1} AaeAPO in distilled water, pH 7. The sample was continuously injected over a timescale of 10 min and eluted with acetonitrile/H_2O 60:40. Eluted substances were detected with a diode array detector (DAD 1100, Agilent) by comparing their UV spectra and retention times with authentic references. ^1H NMR spectra were recorded after incubation of AaeAPO/H_2O_2 with 4MI in D_2O overnight with a 300-MHz NMR spectrometer (Varian MercuryVX 300, Agilent) and compared with the spectra of the authentic references.

RESULTS

Overall Structure of AaeAPO

Two crystal structures were determined at high resolution, termed AaeAPO-MZ0 (for a crystal form obtained at pH 8.5) and AaeAPO-ACT (obtained at pH 4.6). In AaeAPO-MZ0 and AaeAPO-ACT crystals, two and four protein molecules are contained in the asymmetric unit, respectively. The best defined or most complete molecule was the reference for the general structural discussion, as appropriate. The polypeptide contains 328 amino acids, the major part of which are found in helical substructures. However, the first three N-terminal residues are not seen in the crystal structure due to a proteolytic cleavage between Gly-3 and Leu-4 (Fig. 2*A*). This has been verified by N-terminal sequencing. In most cases, the polypeptide is defined from Leu-4 to at least amino acid 326, in one molecule even to the C terminus at position 328. The sequence of the polypeptide matches the cDNA of the corresponding gene *apo1* (39). As with many glycoproteins, both AaeAPO-MZ0 and AaeAPO-ACT have extensively branched carbohydrate chains with up to eight moieties of the high mannose type (40) (Fig. 2*B*). The protein contains one disulfide bridge between Cys-278 and Cys-319, which stabilizes the C-terminal region after the last α-helix. Between Pro-108 and Pro-109, a *cis*-peptide bond was found. Similar to chloroperoxidase, AaeAPO possesses at least one halide binding site (Fig. 2*C*) in the vicinity of the binding pocket entrance of the enzyme. A superpositioning of AaeAPO and CPO shows a large root mean square deviation of about 2.1 Å for 202 common Cα atoms (Fig. 2*D*). Upon closer inspection, it becomes obvious that the structural similarity is restricted to the octahelical core surrounding the heme binding site. In contrast to AaeAPO, the polypeptide of CPO is incomplete relative to the cDNA sequence missing 52 amino acids that are cleaved off during protein maturation (21).

Substrate Binding Pocket and Cation Binding Site

The heme co-factor is embedded within helices with the thiolate sulfur of Cys-36 coordinating to the heme iron at its proximal side at a distance of 2.3 Å. This pattern is attributed to a highly conserved "Peroxidase_2" domain (National Center for Biotechnology Information (NCBI) blastp) characteristic for chloroperoxidases (21, 39). Glu-196 at the distal side of the heme is at an H-bonding distance of ~2.9 Å to Arg-189, thereby forming the acid-base pair required for peroxide cleavage during Compound I formation (Fig. 3*A*) (41).

At one of the heme propionates, a cation binding site very similar to the one in CPO has been identified. In the CPO crystal structure, a manganese cation has been modeled at this site (21, 22) based on its similarity to the cation binding site in manganese peroxidase (42). Strong electron density with 12 σ in a difference map suggested a heavy atom in AaeAPO, but neither x-ray fluorescence spectroscopy of the crystals nor anomalous difference maps indicated the presence of manganese (23). Rather, the heights of residual positive electron density, B-factors, and the coordination geometry of a preliminary refined water molecule suggested a magnesium ion. Furthermore, although refinement of a Mn^{2+} ion resulted in high B-factors and large negative electron density, refining a Mg^{2+}

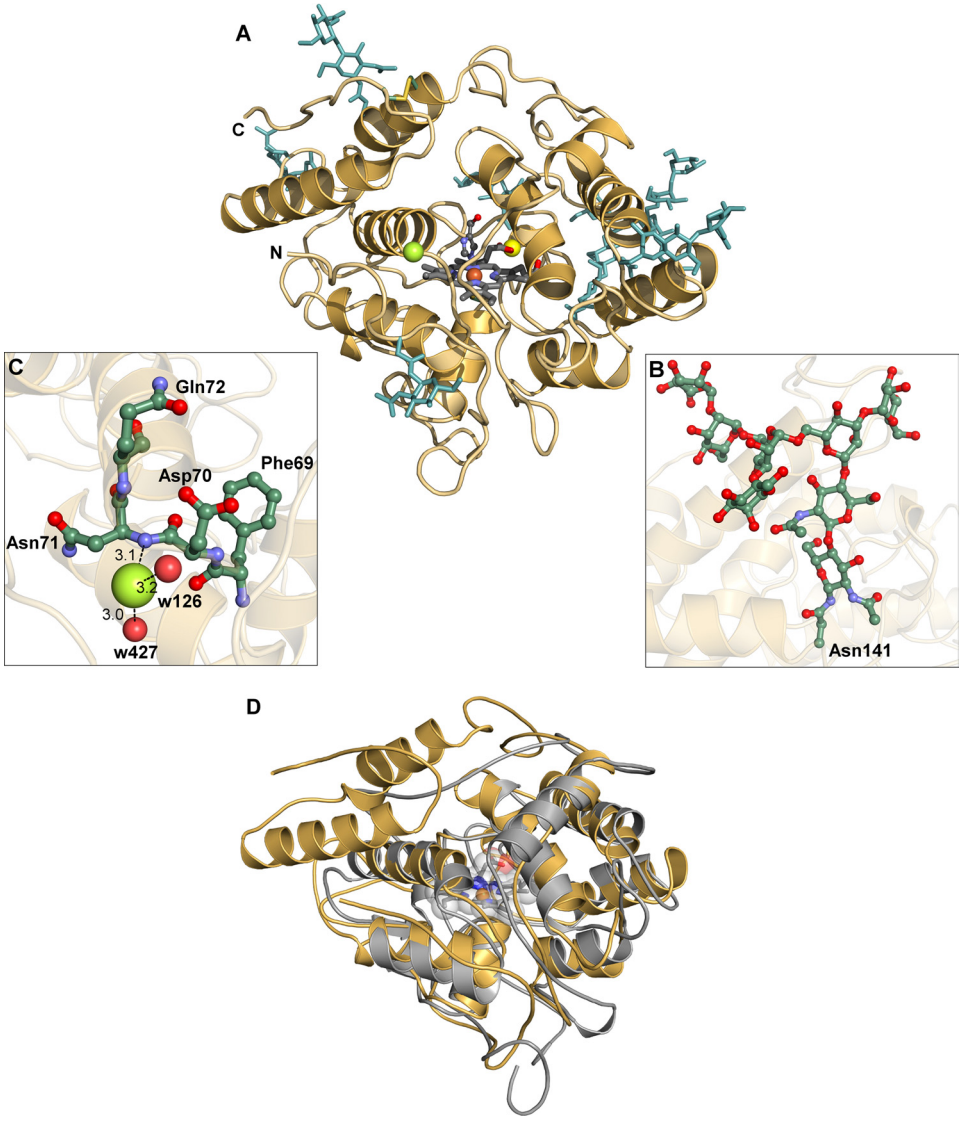

FIGURE 2. **Structural overview and details of AaeAPO.** *A*, ribbon diagram of AaeAPO with the heme, MZ0 (*balls and sticks*), carbohydrates, the chloride anion (*green*), and the disulfide bridge (*yellow sticks*) between Cys-278 and Cys-319. *B*, extensive glycosylation of the high mannose type at Asn-171. *C*, halide binding site with potential hydrogen bonds between chloride and the protein backbone and water molecules. *D*, AaeAPO (*gold*) and CPO (*gray*, PDB code 1CPO) superpositioned by secondary structure matching. The heme is depicted in *sticks* and *transparent space-filling mode*.

ion with full occupancy in both crystal forms yielded reasonable B-factors comparable with the ones of the ligands. The cation has an octahedral coordination with bond lengths (2.1–2.2 Å) as expected for the crystal chemistry of Mg^{2+} (Fig. 3*B*). Mg^{2+} is coordinated by two water molecules and one heme propionate and by three oxygen atoms of the peptide Glu-122–Ser-126 involving hydrogen bonds to Oϵ2 of Glu-122, the backbone carbonyl oxygen of Gly-123, and Oγ of Ser-126. The same binding pattern, including the conserved peptide sequence Glu-*X*-*X*-*X*-Ser, is also found in CPO. To verify the character of the bound cation in AaeAPO, we determined the metal ion contents using ICP-OES and ICP-MS, respectively. With both methods, a slight molar excess relative to heme iron was found for magnesium, whereas only trace amounts of manganese were detectable. These results confirm our crystallographic interpretation that magnesium and not manganese is occupying the cation binding site.

The distal substrate binding pocket is shaped like a cone frustum with a length of about 17 Å and an outer diameter of roughly 10 Å (Fig. 4*A*). At the tip of the cone, defined by the distal Glu-196, three phenylalanines, and one alanine side chain, the diameter is about 8.5 Å. The wall of this cavity is clad by predominantly aromatic and a few aliphatic residues (Fig. 4*B*). Toward the exterior, two polar residues (Ser and Thr) are present, albeit with their hydroxyl groups pointing away from the void. The design of this pocket curiously recalls the pitcher of a *Nepenthes* fly trap (a carnivorous plant).

Binding Modes of Ligands in the AaeAPO Heme Pocket

Acetate—For crystals grown at pH 4.6, the electron density map indicated the presence of a small, planar molecule distal to the heme. Taking into account that the crystallization medium of AaeAPO-ACT contained high concentrations of acetate (23), we assumed that such a molecule was trapped in the heme

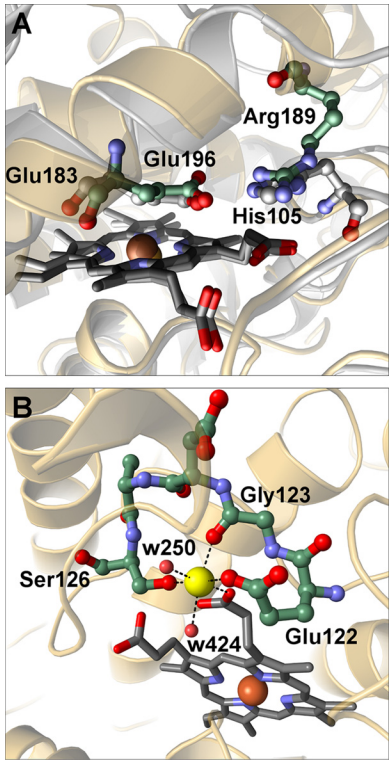

FIGURE 3. **Structural characterization of the distal acid-base pair and the cation binding site.** *A*, overlay of the distal acid-base pair in AaeAPO (*green*) and CPO (*gray*). *B*, the geometry of the cation binding site of AaeAPO containing a magnesium cation (*yellow*). All six Mg^{2+}-O distances are between 2.1 and 2.2 Å. All distances are given in Å.

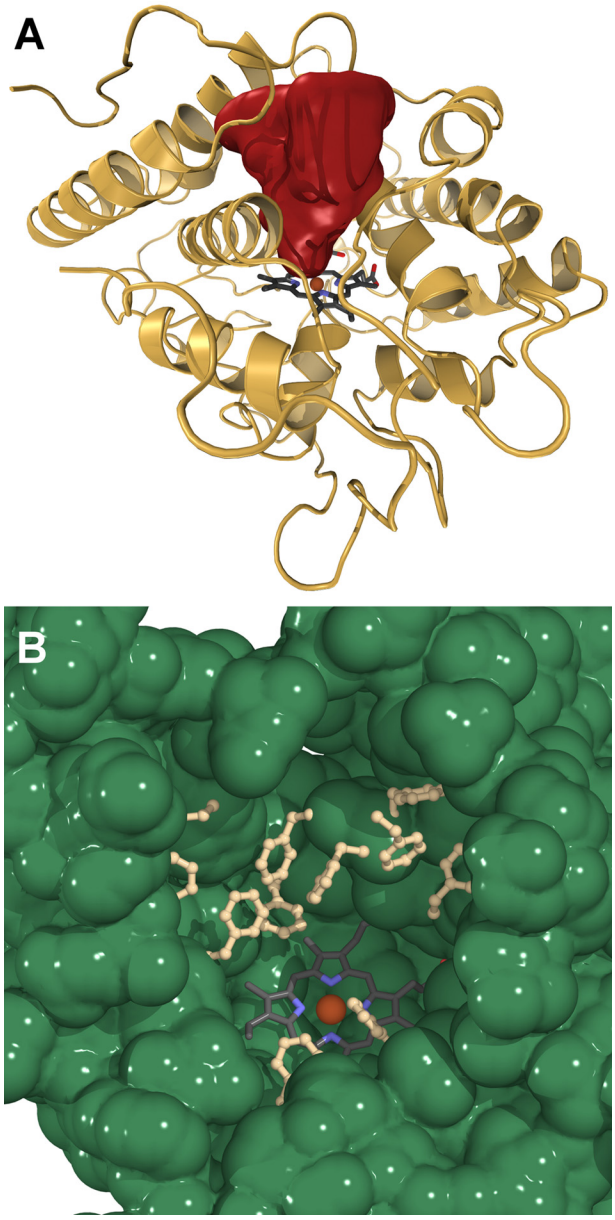

FIGURE 4. **The distal heme-access channel.** *A*, cone-shaped cavity of the substrate oxidation site in AaeAPO. The channel surface is colored in *red*. *B*, distribution of aromatic residues cladding the cavity.

cavity, and refinement indeed proved satisfactory. In all four subunits, the sp^2 plane of acetate lies almost perpendicular to the heme. One carboxyl oxygen points to the entrance of the cavity and forms a hydrogen bond to other surrounding polar atoms. The other oxygen of the carboxylate is in a distance of ~3 Å to the heme iron and thus does not coordinate. This distance between the acetate oxygen and the heme iron might be indicative for a mixed spin state in AaeAPO-ACT as suggested for a CPO-acetate complex (43). The methyl group and the carboxylic C-atom are in van der Waals distance to one pyrrole ring of the heme system, the side chain of Ala-77, and a triad of phenylalanines (Phe 69, Phe-121 and Phe-199) (Fig. 5*A*).

4(5)-(Hydroxymethyl)Imidazole—While commencing with model building of AaeAPO-MZ0, we noticed strong residual electron density (up to 10 σ) located distal to the heme in both subunits. Its size and shape ruled out acetate but rather implied a substituted five-membered heterocyclic ring coordinating to the heme iron. Scrutinizing its chemical environment (polar contacts, hydrogen bonds, and hydrophobic interactions), we eventually identified the bound molecule as MZ0 (Fig. 5*B*). The N1 atom of MZ0 is weakly coordinated to the heme iron at a distance of ~2.3 Å. N2 of the imidazole ring, and the hydroxyl group both form strong hydrogen bonds to two water molecules that are part of a water network extending toward the solvent. The aromatic ring is fixed in its position by the above mentioned phenylalanine triad. Due to the equilibrium between two tautomers (Fig. 1), MZ0 is referred to as 4(5)-(hydroxymethyl)imidazole. In AaeAPO-MZ0, however, bound MZ0 can readily be identified as 5-(hydroxymethyl)imidazole because only the unprotonated nitrogen atom is available for complexation with the heme iron.

The question arises whether or not MZ0 can be regarded as the product of a catalytic turnover of AaeAPO with 4MI. We were able to extract this substrate from the soybean meal used as growth medium for *A. aegerita* and to verify its identity by means of electrospray mass ionization-MS. With biochemical assays, we confirmed our crystallographic interpretation that 4MI is hydroxylated by AaeAPO at the methyl group. In other words, 4MI is a substrate of AaeAPO, albeit with a relatively low k_{cat} of 0.96 s^{-1}.

Molecular modeling studies can provide a more detailed picture of the oxyfunctionalization process of hydrocarbons. In a first step, 4MI was introduced as a ligand in a hypothetical AaeAPO Compound I. The geometry of the oxoferryl was

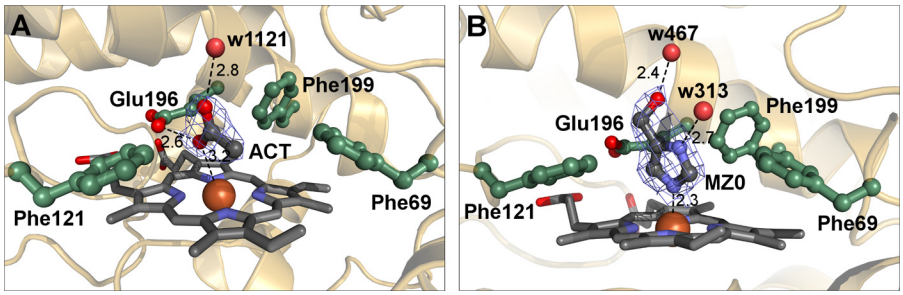

FIGURE 5. **Acetate and MZ0 as heme ligands.** *A*, binding mode of acetate in AaeAPO-ACT. The acetate is displayed with its electron density (difference omit map). *B*, binding mode of MZ0 in the distal side pocket of AaeAPO-MZ0. MZ0 is displayed with its electron density (difference omit map). All distances are given in Å.

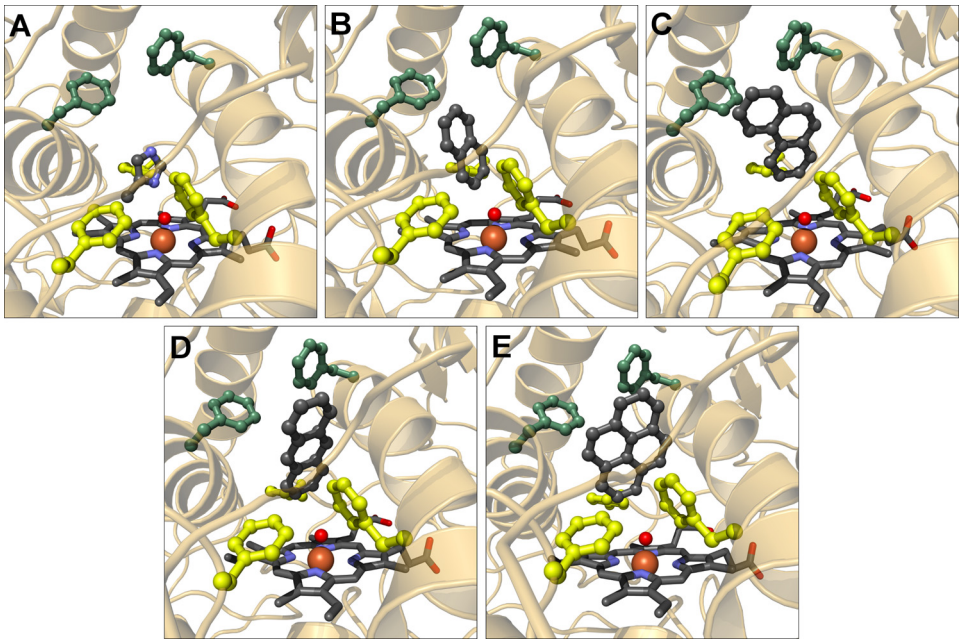

FIGURE 6. **Binding modes of 4MI and several PAHs in AaeAPO.** *A*, complex of AaeAPO and 4MI calculated with Molegro Virtual Docker. The Compound I oxygen is depicted as a *red sphere*. *B–E*, complexes of AaeAPO with naphthalene, phenanthrene, anthracene, and pyrene, respectively. The three Phes colored in *yellow* cooperate in the anchoring and orientation of the aromatic substrate molecules. The *green* Phes impose an upper limit on the longitudinal dimension of the substrates.

assumed to be equivalent to that in a horseradish peroxidase Compound I structure (44). Enzyme-ligand models were calculated using the molecular docking software Molegro Virtual Docker. Indeed, the ligand was placed in a position compliant with hydroxylation at the methyl group (Fig. 6*A*). One nitrogen atom of the ligand is in H-bonding distance with the modeled oxoferryl moiety, with the methyl group in van der Waals distance to this oxygen. The second nitrogen atom points toward the upper end of the pocket, enabling H-bond formation with water molecules. The methyl group is directed toward the hydrophobic lower cavity wall, near Phe-69. A favorable interaction occurs between the aromatic imidazole ring and the aromatic systems of Phe-121 and Phe-199. The planes of the latter are oriented almost perpendicular to the imidazole ring.

Polycyclic Aromatic Hydrocarbons—Several PAHs ranging from a bicyclic (naphthalene) to pentacyclic systems (pentacene and perylene) were analyzed via ligand docking as to how they fit into the heme cavity and are able to occupy a position allowing oxygen transfer from the oxoferryl state of the heme (Fig. 6, *B–E*). Molecular docking yielded plausible enzyme-ligand complexes for all PAHs from a steric viewpoint, except pentacene and perylene. The binding modes for the PAHs are very similar; the aromatic rings come to lie between five phenylalanines (Phe-69, -76, -121, -191, and -199) within the binding pocket (Fig. 6, *B–E*). Atoms C1 and C2 are in van der Waals contact with the oxyferryl heme. This is in accordance with an *ad interim* epoxidation of the C1–C2 bond. Only for the bulkiest inspected ligand, pyrene, some close contacts with the surrounding polypeptide (including Ala-77 and Thr-192) result. A certain degree of flexibility of the protein backbone could readily explain why pyrene is still, although with very low rates, converted to pyrenol by AaeAPO (45). Docking solutions for the two larger and bulkier PAHs show serious clashes with the protein that would require substantial rearrangements of side chains as well as of the backbone. This is in excellent agreement with pentacene and perylene not being converted by AaeAPO.

DISCUSSION

Here we report two structures of AaeAPO with the heme iron in different coordinative environments. Essentially, AaeAPO-MZ0 was crystallized under the same conditions as AaeAPO-ACT, the sole difference being the buffer used for pH adjust-

ment. The question arises why MZ0 is absent from the substrate binding pocket at lower pH. Imidazole has a pK_b value of 6.9 in water and will readily be protonated under more acidic conditions. As a consequence, the coordination bond between the nitrogen atom of the imidazole ring will not be available for coordination to iron anymore. Furthermore, the solubility of protonated MZ0 is increased in aqueous solution when compared with the unprotonated form. A low pH thus liberates MZ0 from the substrate binding pocket. Subsequent formation of AaeAPO-ACT is due to the high concentration of acetate in the crystallization medium. With respect to the presence of MZ0, we suspected the complex cultivation medium as a possible source. 4MI has been shown to occur in many foods, including soy products (and also the soybean meal employed as cultivation medium in this study), due to Maillard reactions during heat processing (46). This has been discussed in context of the carcinogenic properties of 4MI in recent years (24).

Although we have crystallized AaeAPO in complex with a substrate-derived ligand, the structure does not represent an enzyme-substrate complex. Rather, it represents an enzyme-inhibitor complex with an imidazole derivative. Such a binding mode is also observed in the crystal structure of a cytochrome P450-imidazole inhibitor complex (Protein Data Bank (PDB) code 2H7Q) where the imidazole N1 coordinates to the heme iron at a distance of 2.12 Å at pH 7 (47). Like imidazole in the P450 structure, MZ0 forms a hydrogen bond to a water molecule via its N2 and adopts overall a very similar orientation with respect to the heme.

Enzyme assays with $H_2{}^{18}O_2$ have unambiguously proven that the newly introduced oxygen in the APO reaction products originates from peroxide (10). This leaves no doubt that oxygenation must take place in a substrate binding pocket on the distal side of the heme. Because Compound I is a rather short lived intermediate, it cannot be crystallized. As an alternative, we computed Compound I-substrate complexes with several PAHs. An array of five pivotal phenylalanines defines the space available for fitting aromatic substrates in the cavity. Apparently, the phenylalanine triad around the active site fixates the PAHs, whereas the remaining upper two further restrict the substrates in their degrees of freedom and impose an upper limit for the size of molecules to be converted (Fig. 6, *B–E*). This setup is optimally suited for an electrophilic attack of the reactive oxygen species at the C1–C2–π bond resulting in the formation of the epoxide intermediate. Subsequent epoxide ring opening leads to the formation of the hydroxylated products. Although no structural data are available for other APOs yet, a sequence alignment with MroAPO reveals that Phe-69 is replaced by Val-51 and Phe-121 is replaced by Ile-84. It can thus be inferred that MroAPO provides more space around the oxoferryl moiety. In accordance, it has been found that MroAPO catalyzes reactions with bulkier substrates such as steroids and codeines that are not converted by AaeAPO.[5] On the other hand, MroAPO does not display such a high catalytic competence for aromatic compounds (catalytic efficiency and regio- and stereoselectivity), pointing again to the significance of the phenylalanine triad for optimal positioning of aromatic substrates. In other words, the binding pocket is designed for the highly specific and catalytically efficient conversion of arenes.

Despite their structural similarities, AaeAPO and CPO are notably different with respect to their catalytic properties. CPO is the archetypical haloperoxidase, in contrast AaeAPO displays only weak haloperoxidase activity restricted to bromide. The predominant reactivity of the latter is that of a peroxygenase. Naturally, both enzymes have to go through Compound I formation in their catalytic cycles. According to the Poulos-Kraut mechanism, a distal acid-base pair plays a crucial role in this process in all peroxidases (48, 49). In CPO, this pair consists of Glu-183 and His-105, whereas in AaeAPO, the basic part is assumed by Arg-189 (Fig. 3*A*). The two pairs are undoubtedly functionally homologous, but realized in different ways; the two bases are part of spatially unrelated peptides. Nevertheless, the nitrogen atoms of the two basic residues are almost congruent in a superpositioning of AaeAPO and CPO (Fig. 3*A*). It is interesting to note that in an unrelated peroxidase, a similar acid-base pair as in AaeAPO (Asp/Arg) is employed (49). Nature's uncanny ability to achieve the same result in various ways is well demonstrated thereby (50).

With regard to the cation binding site, our results clearly indicate the presence of a magnesium ion in AaeAPO. Only trace amounts of manganese were detected by ICP-OES and ICP-MS. In a survey of all available chloroperoxidase structures, we found that the B-factors of the manganese ions are systematically higher than that of their ligating atoms. This strongly indicates that the binding site is occupied by a cation with a lower atom weight. We thus conclude that the manganese ion has been assigned erroneously in CPO. Probably, and as in AaeAPO, a magnesium ion occupies the CPO cation binding site. Mg^{2+} is redox-inactive and might stabilize the protein structure in a similar way as does Ca^{2+} in lignin peroxidase and other "classical" heme peroxidases (51). Further, no correlation between the presence or absence of manganese and CPO activity has been found (21). From our results, the identity of the metal ion in CPO is still an open matter.

The particular role APOs play in the fungal microcosm is still unknown. It is conceivable that, due to their catalytic versatility and their general abundance in fungi, they are an integral part of an unspecific oxidation and detoxification layout. In the light of this assumed function, APOs may be viewed as a fungal "extracellular liver." Detoxification might also apply to the degradation of defensive compounds synthesized by plants to keep fungal parasites at bay. Because APOs are abundant in saprotrophic species as well, they may also bestow advantages in interspecific competition for carbon sources.

Fungal APOs are very efficient biocatalysts for the oxyfunctionalization of hydrocarbons. Structurally, they moderately resemble the chloroperoxidase CPO, whereas their catalytic scope is akin to cytochrome P450 enzymes. However, in contrast to the latter, they are independent from a cellular environment and require only H_2O_2 as co-substrate and are less prone to catalyst aging. This makes them a potent alternative for typical P450 applications and beyond. This study provides the first structural insights into this group of enzymes and has led to a comprehensive understanding of its catalytic properties. It paves the way

[5] M. Hofrichter, unpublished results.

for the development of a new generation of environmentally friendly oxyfunctionalization catalysts by means of specifically designed APOs, for example through site-directed mutagenesis.

Acknowledgments—We gratefully acknowledge the opportunity to collect diffraction data and thank the staff at beam line ID23-1 of the ESRF for their support.

REFERENCES

1. Arndtsen, B. A., Bergman, R. G., Mobley, T. A., and Peterson, T. H. (1995) Selective intermolecular carbon–hydrogen bond activation by synthetic metal complexes in homogeneous solution. *Acc. Chem. Res.* **28,** 154–162
2. Bard, A. J., Whitesides, G. M., Zare, R. N., and McLafferty, F. W. (1995) Holy Grails in chemistry. *Acc. Chem. Res.* **28,** 91
3. Kakiuchi, F., and Chatani, N. (2003) Catalytic methods for C–H bond functionalization: application in organic synthesis. *Adv. Synth. Catal.* **345,** 1077–1101
4. Bordeaux, M., Galarneau, A., and Drone, J. (2012) Catalytic, mild, and selective oxyfunctionalization of linear alkanes: current challenges. *Angew. Chem. Int. Ed. Engl.* **51,** 10712–10723
5. Munro, A. W., Girvan, H. M., and McLean, K. J. (2007) Variations on a (t) heme – novel mechanisms, redox partners and catalytic functions in the cytochrome P450 superfamily. *Nat. Prod. Rep.* **24,** 585–609
6. Munro, A. W., Girvan, H. M., Mason, A. E., Dunford, A. J., and McLean, K. J. (2013) What makes a P450 tick? *Trends. Biochem. Sci.* **38,** 140–150
7. Guengerich, F. P. (2002) Cytochrome P450 enzymes in the generation of commercial products. *Nat. Rev. Drug Discov.* **1,** 359–366
8. Sakaki, T. (2012) Practical application of cytochrome P450. *Biol. Pharm. Bull.* **35,** 844–849
9. Ullrich, R., and Hofrichter, M. (2007) Enzymatic hydroxylation of aromatic compounds. *Cell Mol. Life Sci.* **64,** 271–293
10. Hofrichter, M., Ullrich, R., Pecyna, M. J., Liers, C., and Lundell, T. (2010) New and classic families of secreted fungal heme peroxidases. *Appl. Microbiol. Biotechnol.* **87,** 871–897
11. Ullrich, R., Nüske, J., Scheibner, K., Spantzel, J., and Hofrichter, M. (2004) Novel haloperoxidase from the agaric basidiomycete *Agrocybe aegerita* oxidizes aryl alcohols and aldehydes. *Appl. Environ. Microbiol.* **70,** 4575–4581
12. Peter, S., Kinne, M., Wang, X., Ullrich, R., Kayser, G., Groves, J. T., and Hofrichter, M. (2011) Selective hydroxylation of alkanes by an extracellular fungal peroxygenase. *FEBS J.* **278,** 3667–3675
13. Churakova, E., Kluge, M., Ullrich, R., Arends, I., Hofrichter, M., and Hollmann, F. (2011) Specific photobiocatalytic oxyfunctionalization reactions. *Angew. Chem. Int. Ed. Engl.* **50,** 10716–10719
14. Gutiérrez, A., Babot, E. D., Ullrich, R., Hofrichter, M., Martínez, A. T., and del Río, J. C. (2011) Regioselective oxygenation of fatty acids, fatty alcohols and other aliphatic compounds by a basidiomycete heme-thiolate peroxidase. *Arch. Biochem. Biophys.* **514,** 33–43
15. Kinne, M., Poraj-Kobielska, M., Ralph, S. A., Ullrich, R., Hofrichter, M., and Hammel, K. E. (2009) Oxidative cleavage of diverse ethers by an extracellular fungal peroxygenase. *J. Biol. Chem.* **284,** 29343–29349
16. Poraj-Kobielska, M., Kinne, M., Ullrich, R., Scheibner, K., Kayser, G., Hammel, K. E., and Hofrichter, M. (2011) Preparation of human drug metabolites using fungal peroxygenases. *Biochem. Pharmacol.* **82,** 789–796
17. Samanta, S. K., Singh, O. V., and Jain, R. K. (2002) Polycyclic aromatic hydrocarbons: environmental pollution and bioremediation. *Trends Biotechnol.* **20,** 243–248
18. Gelboin, H. V. (1980) Benzo[*a*]pyrene metabolism, activation, and carcinogenesis: role and regulation of mixed-function oxidases and related enzymes. *Physiol. Rev.* **60,** 1107–1166
19. Kästner, M., Streibich, S., Beyrer, M., Richnow, H. H., and Fritsche, W. (1999) Formation of bound residues during microbial degradation of [^{14}C]anthracene in soil. *Appl. Environ. Microbiol.* **65,** 1834–1842
20. Gröbe, G., Ullrich, R., Pecyna, M. J., Kapturska, D., Friedrich, S., Hofrichter, M., and Scheibner, K. (2011) High-yield production of aromatic peroxygenase by the agaric fungus *Marasmius rotula*. *AMB Express* **1,** 31
21. Sundaramoorthy, M., Terner, J., and Poulos, T. L. (1995) The crystal structure of chloroperoxidase: a heme peroxidase–cytochrome P450 functional hybrid. *Structure* **3,** 1367–1377
22. Kühnel, K., Blankenfeldt, W., Terner, J., and Schlichting, I. (2006) Crystal structures of chloroperoxidase with its bound substrates and complexed with formate, acetate, and nitrate. *J. Biol. Chem.* **281,** 23990–23998
23. Piontek, K., Ullrich, R., Liers, C., Diederichs, K., Plattner, D. A., and Hofrichter, M. (2010) Crystallization of a 45 kDa peroxygenase/peroxidase from the mushroom *Agrocybe aegerita* and structure determination by SAD utilizing only the haem iron. *Acta Crystallogr. Sect. F Struct. Biol. Cryst. Commun.* **66,** 693–698
24. Chan, P. C., Hill, G. D., Kissling, G. E., and Nyska, A. (2008) Toxicity and carcinogenicity studies of 4-methylimidazole in F344/N rats and B6C3F1 mice. *Arch. Toxicol.* **82,** 45–53
25. Kabsch, W. (2010) *XDS*. *Acta Crystallogr. D Biol. Crystallogr.* **66,** 125–132
26. Kabsch, W. (2010) Integration, scaling, space-group assignment and post-refinement. *Acta Crystallogr. D Biol. Crystallogr.* **66,** 133–144
27. Schneider, T. R., and Sheldrick, G. M. (2002) Substructure solution with *SHELXD*. *Acta Crystallogr. D Biol. Crystallogr.* **58,** 1772–1779
28. Sheldrick, G. M. (2008) A short history of *SHELX*. *Acta Crystallogr. A* **64,** 112–122
29. Vonrhein, C., Blanc, E., Roversi, P., and Bricogne, G. (2007) Automated structure solution with autoSHARP. *Methods Mol. Biol.* **364,** 215–230
30. Abrahams, J. P., and Leslie, A. G. W. (1996) Methods used in the structure determination of bovine mitochondrial F_1 ATPase. *Acta Crystallogr. D Biol. Crystallogr.* **52,** 30–42
31. Cowtan, K. (2006) The *Buccaneer* software for automated model building. 1. Tracing protein chains. *Acta Crystallogr. D Biol. Crystallogr.* **62,** 1002–1011
32. Skubák, P., Murshudov, G. N., and Pannu, N. S. (2004) Direct incorporation of experimental phase information in model refinement. *Acta Crystallogr. D Biol. Crystallogr.* **60,** 2196–2201
33. Emsley, P., and Cowtan, K. (2004) *Coot*: model-building tools for molecular graphics. A*cta Crystallogr. D Biol. Crystallogr.* **60,** 2126–2132
34. McCoy, A. J., Grosse-Kunstleve, R. W., Storoni, L. C., and Read, R. J. (2005) Likelihood-enhanced fast translation functions. *Acta Crystallogr. D Biol. Crystallogr.* **61,** 458–464
35. DeLano, W. L. (2010) *The PyMOL Molecular Graphics System*, version 1.3r1., Schrödinger, LLC, New York
36. Ho, B. K., and Gruswitz, F. (2008) HOLLOW: generating accurate representations of channel and interior surfaces in molecular structures. *BMC Struct. Biol.* **8,** 49
37. Thomsen, R., and Christensen, M. H. (2006) MolDock: a new technique for high-accuracy molecular docking. *J. Med. Chem.* **49,** 3315–3321
38. Casal, S., Fernandes, J. O., Oliveira, M. B. P. P., and Ferreira, M. A. (2002) Gas chromatographic–mass spectrometric quantification of 4-(5-)-methylimidazole in roasted coffee after ion-pair extraction. *J. Chromatogr. A* **976,** 285–291
39. Pecyna, M. J., Ullrich, R., Bittner, B., Clemens, A., Scheibner, K., Schubert, R., and Hofrichter, M. (2009) Molecular characterization of aromatic peroxygenase from *Agrocybe aegerita*. *Appl. Microbiol. Biotechnol.* **84,** 885–897
40. Kornfeld, R., and Kornfeld, S. (1985) Assembly of asparagine-linked oligosaccharides. *Annu. Rev. Biochem.* **54,** 631–664
41. Wang, X., Peter, S., Kinne, M., Hofrichter, M., and Groves, J. T. (2012) Detection and kinetic characterization of a highly reactive heme-thiolate peroxygenase Compound I. *J. Am. Chem. Soc.* **134,** 12897–12900
42. Sundaramoorthy, M., Kishi, K., Gold, M. H., and Poulos, T. L. (1994) The crystal structure of manganese peroxidase from *Phanerochaete chrysosporium* at 2.06-Å resolution. *J. Biol. Chem.* **269,** 32759–32767
43. Sono, M., Dawson, J. H., Hall, K., and Hager, L. P. (1986) Ligand and halide binding properties of chloroperoxidase: peroxidase-type active site heme environment with cytochrome P-450 type endogenous axial ligand and spectroscopic properties. *Biochemistry* **25,** 347–356
44. Berglund, G. I., Carlsson, G. H., Smith, A. T., Szöke, H., Henriksen, A., and Hajdu, J. (2002) The catalytic pathway of horseradish peroxidase at high

resolution. *Nature* **417,** 463–468
45. Aranda, E., Ullrich, R., and Hofrichter, M. (2010) Conversion of polycyclic aromatic hydrocarbons, methyl naphthalenes and dibenzofuran by two fungal peroxygenases. *Biodegradation* **21,** 267–281
46. Moon, J.-K., and Shibamoto, T. (2011) Formation of carcinogenic 4(5)-methylimidazole in Maillard reaction systems. *J. Agric. Food. Chem.* **59,** 615–618
47. Verras, A., Alian, A., and Ortiz de Montellano, P. R. (2006) Cytochrome P450 active site plasticity: attenuation of imidazole binding in cytochrome $P450_{cam}$ by an L244A mutation. *Protein Eng. Des. Sel.* **19,** 491–496
48. Poulos, T. L., and Kraut, J. (1980) The stereochemistry of peroxidase catalysis. *J. Biol. Chem.* **255,** 8199–8205
49. Strittmatter, E., Liers, C., Ullrich, R., Wachter, S., Hofrichter, M., Plattner, D. A., and Piontek, K. (2013) First crystal structure of a fungal high-redox potential dye-decolorizing peroxidase. Substrate interaction sites and long-range electron transfer. *J. Biol. Chem.* **288,** 4095–4102
50. Gherardini, P. F., Wass, M. N., Helmer-Citterich, M., and Sternberg, M. J. E. (2007) Convergent evolution of enzyme active sites is not a rare phenomenon. *J. Mol. Biol.* **372,** 817–845
51. Choinowski, T., Blodig, W., Winterhalter, K. H., and Piontek, K. (1999) The crystal structure of lignin peroxidase at 1.70 Å resolution reveals a hydroxy group on the Cβ of tryptophan 171: a novel radical site formed during the redox cycle. *J. Mol. Biol.* **286,** 809–827